Ultralow Secondary Electron Emission of Graphene

Jun Luo,[†,*] Peng Tian,[‡] Cheng-Ta Pan,[§] Alexander W. Robertson,[†] Jamie H. Warner,[†] Ernie W. Hill,[‡] and G. Andrew D. Briggs[†]

[†]Department of Materials, University of Oxford, Parks Road, Oxford OX1 3PH, United Kingdom, [‡]School of Computer Science, University of Manchester, Kilburn Building, Oxford Road, Manchester M13 9PL, United Kingdom, and [§]School of Physics and Astronomy, University of Manchester, Oxford Road, Manchester M13 9PL, United Kingdom

ABSTRACT In order to ensure that vacuum electronic devices work with high overall efficiency, it is required to use materials with low secondary electron emission to fabricate or coat collectors, grids, and envelope walls of the devices. We report that the secondary electron yields of monolayer graphenes are ultralow, comparable with the lowest yields of the materials currently used in this practical application. This offers a pathway for the application of light graphene with only one-atom thickness and good electronic and thermal conductivities in vacuum electronic devices.

KEYWORDS: graphene · monolayer · secondary electron emission · secondary electron yield · scanning electron microscopy

Graphene has been found to possess remarkable electronic,[1−8] mechanical,[9,10] and thermal properties[11] and so is believed to have potential applications in many different fields ranging from electronics to energy conversion.[1−12] Here, we show a new intrinsic property of graphene, ultralow secondary electron (SE) emission, which is crucial for ensuring that vacuum electronic devices are able to work with high overall efficiency. A vacuum electronic device consists of several electrodes sealed in an insulating envelope and is used to create, switch, modify, or amplify an electrical signal by controlling the action of electrons in vacuum. These types of devices are widely used in communication, radar, guidance, space probes, and heating. For example, a traveling wave tube enables communication satellites to transmit television signals from space directly to private houses.[13,14] In order to enhance the overall efficiency of vacuum electronic devices, it is required to suppress the SE emission from the collector electrodes of the devices.[13−15] Also, the SE emission from the grids and the envelope walls of the devices needs to be low for preventing radio frequency (rf) vacuum breakdown in the devices.[16] At present, the material most widely used in industry for fabricating or coating the collectors, the grids, and the envelope walls is ion-textured graphite, whose SE yield is about 0.2 and the lowest in the working environment of the devices.[13,14]

We find experimentally that the intrinsic SE yields of monolayer graphene are around 0.10, comparable with that of the ion-textured graphite. Moreover, no post-treatment is needed for clean graphene to obtain such low SE yields, whereas ion sputtering is required to produce texture on the graphite for its low SE yield.[13] This opens a new potential application for graphene. Graphene is light, is only one atom thick, and has good thermal and electrical conductivities, which meet the severe requirements of communication and space probes in terms of weight, volume, and power consumption of the vacuum electronic devices.

RESULTS AND DISCUSSION

Figure 1 shows an optical image of a graphene flake on a silicon substrate whose oxide surface layer is 300 nm thick. It is seen that several regions with different contrasts exist in this flake, indicating that these regions have different thicknesses.[17,18] The contrast of the region labeled by A (referred to as region A) is the lowest, and so this region is possibly monolayer graphene. Region B, with the second lowest contrast, is possibly a bilayer. In order to confirm this, Raman spectra were taken from the two regions and are shown in Figure 2.

Figure 2a and b show that the Raman spectra from regions A and B have peaks of the G and G′ bands. The G′ band has been proven to be very sensitive to the number of layers of graphene and can be used to determine the number of layers.[17−20] The G′ peak from region A is sharp, with a fwhm (full width at half-maximum) of 26.8 cm^{-1}; it is symmetric and can be fitted by a single Lorentzian peak with the position at

*Address correspondence to jun.luo@materials.ox.ac.uk.

Received for review September 29, 2010 and accepted January 10, 2011.

Published online January 24, 2011
10.1021/nn102579f

© 2011 American Chemical Society

2673.43 ± 0.07 cm^{-1}. These are characteristic of monolayer graphene. The G′ peak from region B is broad, with a fwhm of 53.5 cm^{-1}; it is asymmetric and can be fitted by four Lorentzian peaks with the positions at 2650.3 ± 0.5, 2683.6 ± 0.3, 2702.7 ± 0.3, and 2717.5 ± 0.6 cm^{-1}. These are characteristic of bilayer graphene. These results confirm that the numbers of layers of regions A and B are correctly determined with the optical microscope. In the following content, all of the monolayer graphenes were identified by the above methods.

Scanning electron microscopy (SEM) has been demonstrated to be able to measure the SE yields of carbon nanotubes (CNTs) in our previous work.[21] Here, we also use SEM to measure the SE yields of monolayer graphene. Our previous work has indicated that the SE measurement requires samples to be connected with electrodes that are used to supply electrons for replenishing the electrons of the samples lost in their SE emission process.[21] Thus, we used lithography to produce electrodes on each graphene flake before any SEM characterization. Figure 3a and b shows an SEM image and Raman spectrum of a graphene flake (referred to as G1) after the lithography and before the SE measurement. The G′ band of Figure 3b is enlarged in Figure 3c and seen to have the same shape as that of Figure 2c, indicating that G1 is monolayer. It should be noted that the lithography could cause the substrate with G1 to be covered by residual resist, and this might influence the SE measurement. Irradiation by an electron beam with the energy of 80 keV in a transmission electron microscope is able to remove a monolayer in few-layer graphene sheets.[10] To remove residual resist from our graphene, if any, and not to destroy the graphene, we used the electron beam with lower energy, 1 keV, in our SEM to irradiate some areas on G1 by using a slow scanning speed and high magnification to give a large integrated exposure. The rectangles with darker contrast on G1, such as M, N, X, Y, U, and W in Figure 3d, are the areas that have been scanned under the high magnification. The darker contrast could be caused by contamination or positive charging on the sample.[22] If it was the positive charging that caused the darker contrast, the darker contrast would disappear after the illumination of the electron beam on the sample is stopped for a time and then the sample is reviewed. Darker contrast caused by contamination would not disappear. Figure 3d was taken after the illumination of the electron beam was stopped for 21 h. Therefore, it is concluded that the darker contrast was caused by contamination.

We used Raman spectroscopy and an atomic force microscope (AFM) to check the effect of the irradiation of the electron beam on G1 and the contamination.

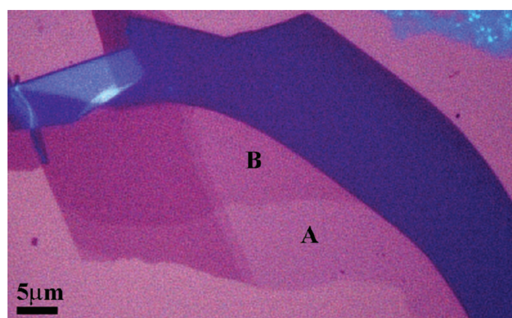

Figure 1. Optical image of a graphene flake on a silicon substrate.

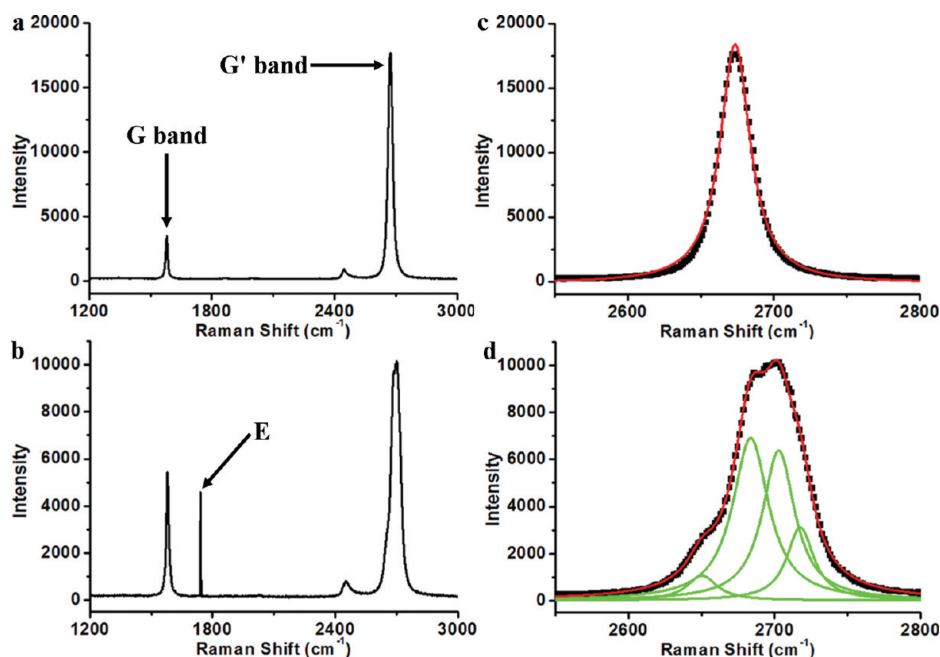

Figure 2. Raman spectra of regions A (a) and B (b) of the graphene flake in Figure 1. The G′ band features in (a) and (b) are enlarged in (c) and (d), respectively, where the solid squares represent the experimental Raman data. The red line in (c) and the green lines in (d) are the Lorentzian peaks used to fit the Raman data. The red line in (d) is the sum of the four green Lorentzian peaks. The line labeled by E in (b) is an artifact introduced by the Raman spectrometer.

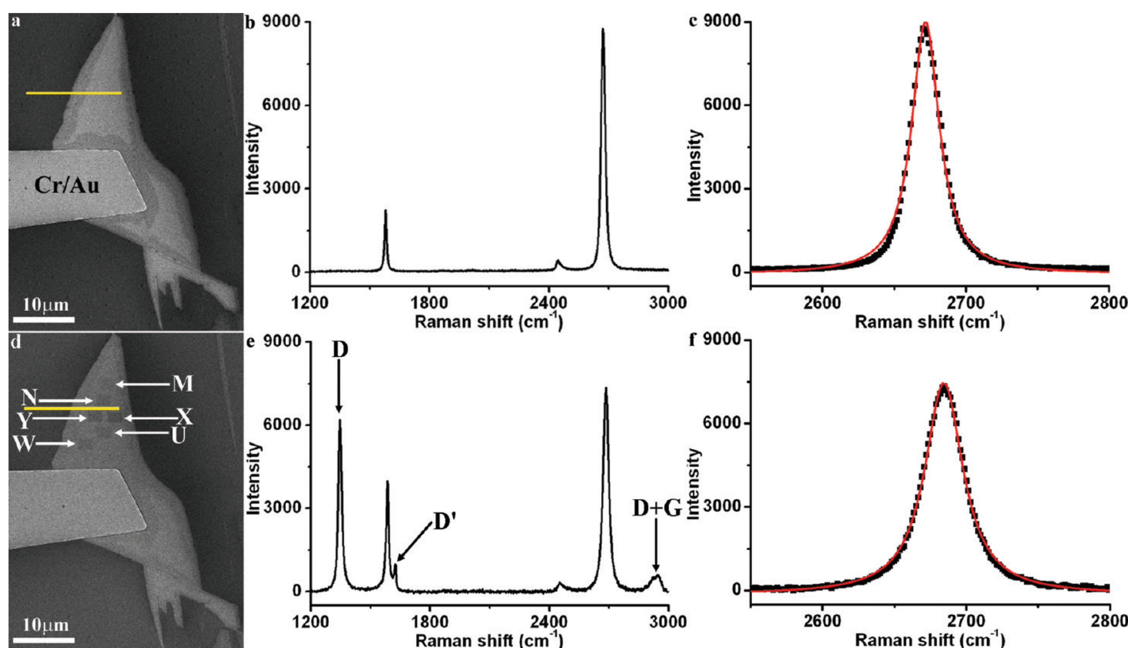

Figure 3. SEM characterization and Raman spectra of a monolayer graphene (referred to as G1) attached with a Cr/Au electrode. (a, b) SEM image and Raman spectrum taken before the SE measurement was performed and the connection between G1 and ground was broken. (c) Enlargement of the G′ peak in (b) with its Lorentz fit in red. (d, e) SEM image and Raman spectrum taken after the SE measurement and the breaking of the grounding connection. (f) Enlargement of the G′ peak in (e) with its Lorentz fit in red. The yellow lines in (a, d) denote the positions to take the profiles in Figure 7.

The Raman spectrum in Figure 3e was taken when the laser spot with a diameter of about 3 μm was focused on the region of Y in Figure 3d. Compared with Figure 3b, three new peaks appear at 1346, 1624, and 2935 cm^{-1}. It has been indicated that the three peaks correspond to the bands of D, D′, and D+G, respectively, and are relevant to defects in monolayer graphene.[23] This implies that defects were produced in G1 by the irradiation of the electron beam. The sharp G and G′ peaks still exist in Figure 3e, and the G′ peak is still symmetric and can be fitted by only one Lorentzian peak, as shown in Figure 3f, indicating that the mainframe of the monolayer graphene was kept. The influence of the defects on the SE yields of the graphene will be discussed later.

Figure 4a and b shows the AFM images of G1 with its surroundings, demonstrating that the rectangles of X, Y, U, and W in Figure 3d are actually pits. The pits of V, Z, and the others on the oxide region outside G1 were produced by the irradiation with the same conditions as those of X, Y, U, and W. The reason that they cannot be seen in Figure 3d is that the contrast of the oxide region was too dark. The depths of the pits of X, Y, and Z are measured to be 0.88 $\pm$ 0.34, 0.75 $\pm$ 0.35, and 0.44 $\pm$ 0.38 nm, respectively, by the height profile in Figure 4c. The heights of the bottoms of the pits of X and Y relative to the bottom of the Z pit are measured to be 0.33 $\pm$ 0.29 and 0.47 $\pm$ 0.30 nm, respectively. The two values are both very close to the thickness of monolayer graphene within the error bars. In total, the bottom heights of the pits of X, Y, and U on G1 relative to the bottoms of V and Z on the oxide are all measured, and their average is 0.37 $\pm$ 0.18 nm, very close to the thickness of monolayer graphene. This consistency between the bottom heights and the monolayer-graphene thickness is also observed in other samples, G2−4 (see details in the Supporting Information). Thus, we can conclude that G1 and its surrounding oxide were covered by a layer of residual resist, and the scanning of the electron beam on the rectangles of X, Y, U, V, and Z cleaned the resist and exposed the surfaces of G1 and the oxide in the corresponding regions. In contrast, the pits of M and N in Figure 4a are too shallow to see. This is because the cleaning ability of the electron beam with lower current is weaker, and the beam current used to scan the rectangles of M and N in Figure 3d was 37.4 pA and much lower than those, 208.5−225.1 pA, for X, Y, U, W, Z, V, and the other visible pits. It was also found that when the current was increased to 40.1−40.7 pA, pits were still shallow but visible (see details in the Supporting Information). Therefore, in order to avoid the influence of the resist, only the SE measurements performed with large electron beam currents will be discussed here. In addition, Figure 4 indicates that the darker edge of G1 in Figure 3a corresponds to the thicker parts of the residual resist. The darker edges were not used for the SE measurement. The formation mechanism of the darker rectangles discussed in the above is different from the one on CNTs in our previous work (see details in the Supporting Information). Raman spectroscopy was also performed on the pit regions on the oxide outside G1, and no signals were detected, indicating that the scanning of

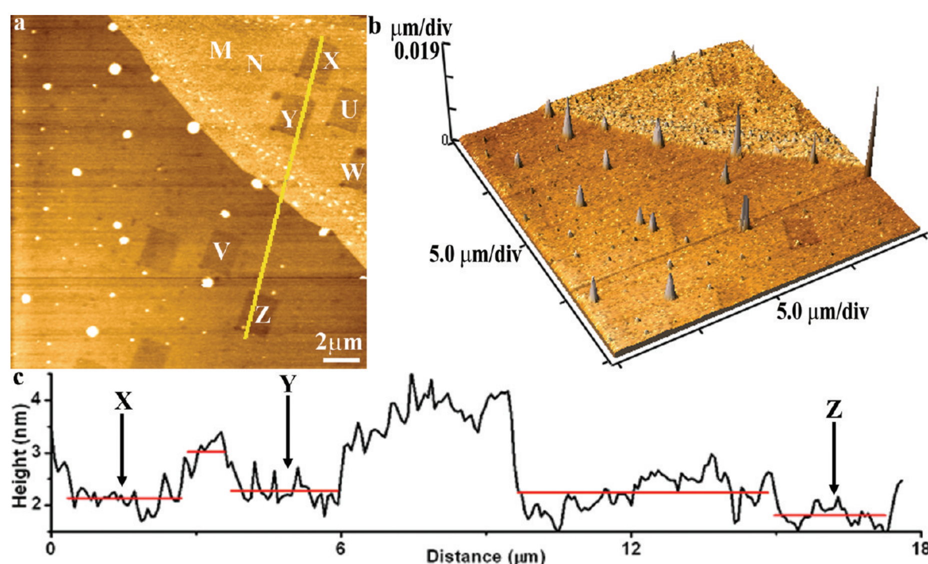

Figure 4. AFM characterization on G1 after Figure 3d was obtained. (a) Two-dimensional (2D) AFM image of G1 with its surroundings. The positions of M, N, X, Y, U, and W are also labeled in Figure 3d. (b) Three-dimensional (3D) AFM image corresponding to (a). (c) Height profile taken from the yellow line in (a), where the red lines present the average heights in the corresponding regions.

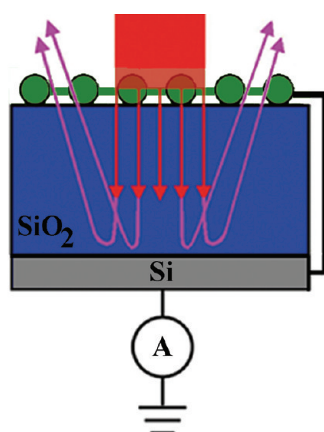

Figure 5. Schematic image of the cross section of G1 interacting with the electron beam. The red and the pink arrows denote the electron beam and backscattered electrons, respectively. The object in green denotes the graphene, which is electrically connected to the conductive Si part of the substrate by the Cr/Au electrode. The Si part is connected with a current meter.

the electron beam here did not induce considerable decomposition of residual hydrocarbon gases under vacuum to produce amorphous carbon. This is because the energy of the electron beam was consumed by its drilling in the residual resist as well as its interaction with the substrate and G1, and so insufficient energy was left to induce the decomposition.

On the basis of the above analysis, Figure 5 depicts the interaction between G1, the substrate, and the electron beam, when the electron beam with large current scans an area fully covered by a part of G1 under high magnification. G1 is very thin and light, and so the high-energy electron beam penetrates through them without much backscattering. However, a portion of the incident electrons will be backscattered by the oxide, as shown by the pink arrows in Figure 5. Both the electron beam and the backscattered electrons (BSEs) can excite the bombarded samples to emit SEs.[24,25] The residual resist is also very thin and light and so cannot backscatter the incident electrons. It could also emit SEs and thus carry positive charges. But, even if this is true, its SEs do not need to be considered, because the resist is removed from the scanned region and its positive charges equal the number of SEs emitted by it, meaning that its removal causes only zero charge in sum to be lost. This is the reason that no resist is mentioned in Figure 5. Thus, for the scanning process in Figure 5, the current balance gives[22,26]

$$I_b = I_{SE} + I_{BSE} + i + C\frac{\Delta E_{surface}}{\Delta t} \quad (1)$$

$$I_{SE} = \delta_{SiO2} I_b + \delta_G (I_b + I_{BSE}) \quad (2)$$

$$I_{BSE} = \eta_{SiO2} I_b \quad (3)$$

$$i = \frac{E_{surface}}{R} = \frac{E_G + E_{SiO2-G}}{R} \quad (4)$$

I_b, I_{SE}, and I_{BSE} denote the currents of the electron beam, the SEs, and the BSEs, respectively. i denotes the leakage current flowing from the scanned area through the samples to ground. The term $C\Delta E_{surface}/\Delta t$ in eq 1 represents a type of charging current and can be neglected unless the scanning rate is very high (the so-called TV rate).[22] Thus, it is neglected here because the scanning speed in our work is much slower than the TV rate (see details in the Experimental Section). δ and η denote the SE and the BSE yields, respectively. G denotes graphene. E_G and $E_{SiO2\text{-}G}$ are the potentials of the scanned graphene and the oxide layer underneath the scanned graphene, respectively,

and their sum is the surface potential $E_{surface}$ in the scanned region. R is the effective leakage resistance between the scanned region and ground. If the electron beam scans an area with the same dimensions as before and without graphene, I_{SE} becomes

$$I'_{SE} = \delta_{SiO2} I_b \quad (5)$$

In the absence of graphene, the leakage current is

$$i' = \frac{E_{SiO2}}{R'} \quad (6)$$

.E_{SiO2} is the potential of the scanned oxide, and R' is the corresponding effective leakage resistance between the scanned oxide and ground. I_b and I_{BSE} are unchanged during the scanning on the two areas with and without the graphene, and so δ_G is given by

$$\delta_G = \frac{i' - i}{I_b(1 + \eta_{SiO2})} \quad (7)$$

. The application of eqs 1−234567 has four conditions: the scanning speed of the electron beam should be slower than the TV scanning speed;[22] a part of the measured graphene should cover fully the scanned area, when i is measured (otherwise, a fractional coefficient would appear in the equations); I_b should be large enough to clean the residual resist; the values of a pair of i' and i used to calculate a value of δ_G should be measured when the value of I_b is fixed. In addition, eq 6 indicates that when $i' \neq 0$, the potential E_{SiO2} in the scanned oxide surface is nonzero. Though the oxide region scanned for measuring i' is outside the graphene region for i, the oxide layer underneath the graphene region could also carry a potential, namely, $E_{SiO2\text{-}G}$ in eq 4, because the graphene is too thin and so the electron beam can penetrate through the graphene and into a range in the oxide layer. Due to the good conduction of the graphene, some of the charge in the oxide layer under the graphene could be transported away, when $E_{SiO2\text{-}G}$ is originally nonzero, and so finally $|E_{SiO2\text{-}G}| \leq |E_{SiO2}|$. The potential of $E_{SiO2\text{-}G}$ is external to the graphene and could affect the SE emission from the graphene. Thus, if we want to measure the intrinsic SE yields of graphene, it is required to ensure $E_{SiO2\text{-}G} = 0$. Since $|E_{SiO2\text{-}G}| \leq |E_{SiO2}|$, $E_{SiO2\text{-}G} = 0$ when $i' = 0$ and $E_{SiO2} = 0$. $E_{SiO2} = E_{SiO2\text{-}G} = 0$ means that the charging and the discharging reach a balance, and so no continuous charge accumulation occurs in the oxide layers. Thus, the SE measurement is unaffected by charging when the measurements of i and i' are performed during the continuous scanning of the electron beam on the graphene and the oxide, as in our experimental process.

All of the measurements shown here met the above five conditions (see details in Table 1 and Experimental Section), except that $i' \neq 0$ when G4 was not connected with ground. In general, I_b can be measured by a Faraday cup and the current meter shown in Figure 5.

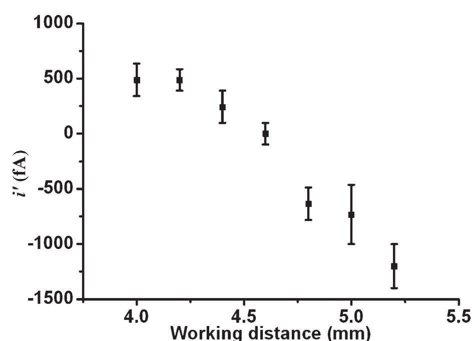

Figure 6. Dependence of the leakage current i' on the working distance, when oxide regions on the substrate of G1 were scanned under the same conditions as those to produce the Z pit in Figure 4a.

i' and i can be measured by the current meter. The values of η_{SiO2} have been measured and listed in a renowned database.[27] At the start of the measurement on each sample, we need to find the experimental condition satisfying $i' = 0$. It is found that changing the working distance in our SEM can change the value of i' when the other experimental conditions are fixed. Figure 6 shows the dependence of i' through the oxide layer of the substrate of G1 on the working distance. It is seen that when the working distance was 4.6 mm, $i' = 0$. Thus, the intrinsic SE yield of G1 was measured with the working distance fixed at 4.6 mm and found to be 0.14 ± 0.01. The corresponding measured data are listed in Table 1.

After this SE measurement, the connection between the electrode on G1 and the ground was broken, and then it was found that the SE yield of G1 dropped to 0.007 ± 0.003, shown in Table 1. The same phenomenon has been reported with diamond and CNT.[16,21] This is because G1 was no longer connected with the ground, and so electrons lost in its SE emission process were unable to be replenished. Thus, G1 became positively charged. The positive charges on G1 generated attraction forces on the SEs emitted by G1 and so limited the ability of G1 to emit SEs further. Because any intrinsic graphene is neutral and positively charging is not intrinsic for graphene, the dropped SE yield, 0.007 ± 0.003, should not be considered as an intrinsic yield of the graphene. In addition, when the unremoved parts of the residual resist and G1 were scanned together under low magnification, the positive charges on G1 were also able to generate attraction forces on the SEs emitted by the unremoved resist parts and then their SE yields also dropped. Since SEM images are formed by the SE signals emitted by samples, the breaking of the grounding connection should cause the contrast of the SEM image of G1 with the unremoved resist parts on it to change. This is confirmed by Figure 3a and d, which shows that the contrast of the G1 area relative to the surrounding oxide before the breaking is higher than that after the breaking. The values of the contrasts before and after the breaking

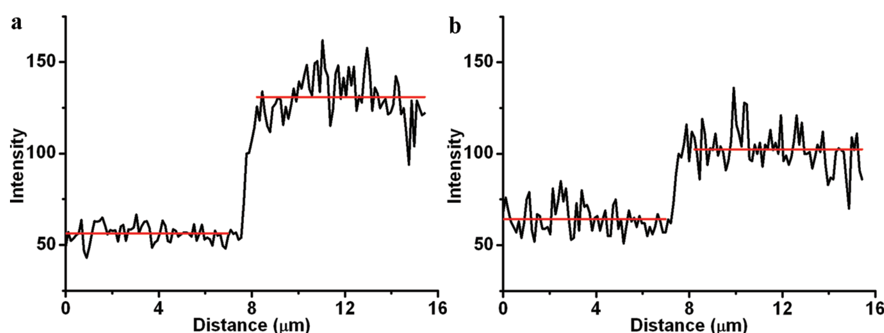

Figure 7. Signal intensity profiles in (a) and (b) taken along the yellow lines in Figure 3a and d, respectively. The red lines are the average values of the intensities in the corresponding regions. The yellow line in Figure 3d is located between the rectangles of N, X, and Y and does not overlap them.

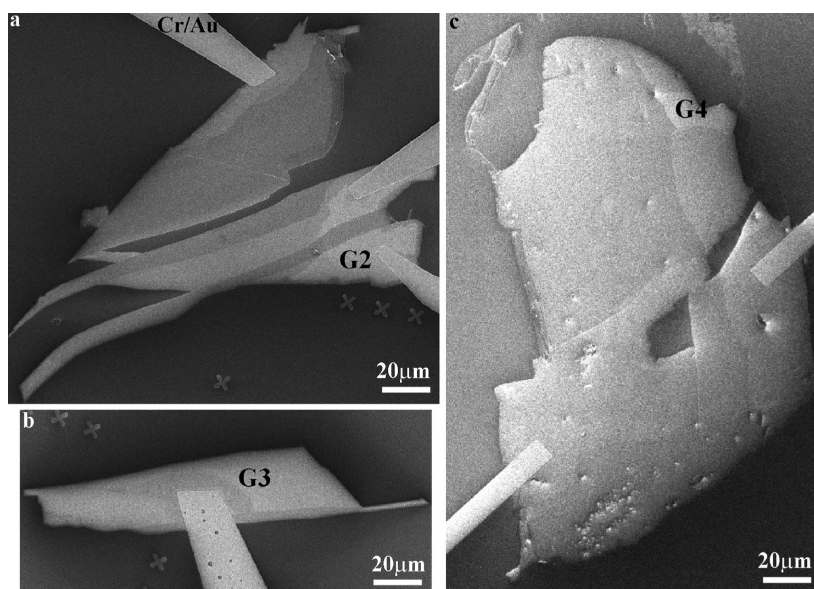

Figure 8. SEM images of the flakes of G2−4. In (a) and (c), only the bright areas indicated by G2 and G4 are the monolayer graphenes used in our work. The whole flake in (b) is monolayer.

are found to be 2.3 ± 0.3 and 1.6 ± 0.3, respectively, by calculating the ratios between the average signal intensities of the corresponding regions in the signal intensity profiles of Figure 3a and d, which are shown in Figure 7a and b.

The above experiments and analyses were repeated on another three sheets of monolayer graphene, G2−4, whose SE measurement data are listed in Table 1, and SEM images are shown in Figure 8 (see their Raman spectra and AFM images in the Supporting Information). The intrinsic SE yields of G2−4 were measured to be 0.08 ± 0.02, 0.093 ± 0.006, and 0.10 ± 0.01, respectively. The three yields and the one of G1, 0.14 ± 0.01, are all close to their average yield, 0.10. All of the SE measurements in this work were done when the energy of the electron beam was 1 keV, which was in the middle of the energy range for measuring the SE yields of the ion-textured graphite.[13] We can see that the range of the intrinsic SE yield of the graphene is comparable with the lowest SE yield of the ion-textured graphite, about 0.2. But a post-treatment of ion sputtering used to produce textures on the graphite is necessary for the low SE yield of the graphite.[13] No post-treatment is needed for clean graphene to obtain such low SE yields. This would be a benefit for the potential application of graphene in this field.

The SE yields of G2−4 also dropped to 0.020 ± 0.007, 0.022 ± 0.006, and −0.144 ± 0.009, respectively, after their electrical connections with the ground were broken. The dropped SE yield of G4 is negative and different from those of G1−3. Before this is discussed, it should be noted that the leakage current, i', corresponding to this negative yield was negative and far away from the zero point of the current meter when oxide regions besides G4 were scanned. This means that negative charges induced by the electron beam irradiation were accumulated in the oxide surface.[22,26] Originally we tried to find a condition corresponding to no charge accumulation. However, the oxide surface of this substrate was charged so heavily that we did not find any condition for no charge accumulation. However, the negatively charged oxide surface underneath G4 was

TABLE 1. Data of the SE and Raman Measurements of Graphene[a]

graphene no.	i' (fA)	i (fA)	I_b (pA)	δ_G	contrast in SEM	connected with ground	I_D/I_G
G1	49 ± 49	$37\,100 \pm 2500$	-208.5 ± 0.5	0.14 ± 0.01	2.3 ± 0.3	yes	1.66
G1	0 ± 98	2100 ± 900	-225.1 ± 1.0	0.007 ± 0.003	1.6 ± 0.3	no	
G2	-49 ± 49	$20\,200 \pm 4300$	-195.8 ± 1.0	0.08 ± 0.02	3.4 ± 0.4	yes	0.85
G2	0 ± 49	5500 ± 2000	-221.2 ± 1.0	0.020 ± 0.007	3.0 ± 0.4	no	
G3	49 ± 49	$24\,600 \pm 1600$	-210.5 ± 0.9	0.093 ± 0.006	3.5 ± 0.6	yes	0.72
G3	49 ± 49	6000 ± 1600	-220.7 ± 0.5	0.022 ± 0.006	2.9 ± 0.6	no	
G4	0 ± 98	$34\,000 \pm 4000$	-260.5 ± 0.7	0.10 ± 0.01	1.9 ± 0.3	yes	1.66
G4	$-17\,000 \pm 2000$	$-64\,000 \pm 2000$	-261.2 ± 1.0	-0.144 ± 0.009	1.2 ± 0.1	no	

[a] The zero point of the current meter is 0 ± 98 fA. All of the SE measurements were done under the irradiation of the electron beam with the energy of 1 keV. The database in ref 27 indicates that η_{SiO2} is 0.25 under this condition. The values of i' and i shown in each subrow were both measured when the value of I_b was fixed at the value shown in the same subrow. The contrast values are from low-magnification SEM images. The values of I_D/I_G are from the Raman spectra measured after the SE measurements.

advantageous for G4 to emit SEs, because the repulsion force existing between the negative charged oxide surface and negative SEs was able to repel the SEs away from G3.[28] Therefore, if the oxide surface was not charged, the SE yield of G4 would be lower than −0.144 and still negative. The negative SE yield of G4 means that a part of the SEs emitted by the oxide layer underneath G4 was screened by G4, which was like a metallic web covering the oxide surface. The reason that this effect was not obvious in the cases of G1−3 is possibly that the total area of the flake containing G4 is much larger than those of G1−3, as shown in Figures 8 and 3a. Therefore, it is concluded that graphene flakes with large areas are a promising candidate to coat the insulating envelope walls of vacuum electronic devices and reduce their SEs. The SEM contrast change was also observed on G2−4, as shown in Table 1 (see details in the Supporting Information).

As mentioned before, defects were introduced into the graphene during the SE measurements. It has been found that the ratio of the intensity of the D peak relative to that of the G peak, namely, I_D/I_G, in the Raman spectrum can be used to quantify defects in graphene.[23] The values of I_D/I_G from the Raman spectra of G1−4 taken after the SE measurements are listed in Table 1. It is seen that the SE yields of G1 and G4 with higher I_D/I_G are 0.14 ± 0.01 and 0.10 ± 0.01, larger than those of G2 and G3 with lower I_D/I_G, 0.08 ± 0.02 and 0.093 ± 0.006. This implies that defects are advantageous to the SE emission of graphene. This is similar to the case of CNTs.[21]

The ultralow SE emission of graphene is in remarkable contrast to the ultrahigh SE emission of CNTs.[21] This difference should be due to the modulation of the electronic structure of CNTs induced by extra electrons in the CNTs. It has been suggested that when an electron beam passes a CNT, the system consisting of the CNT and the electron beam can be considered as the CNT charged with extra electrons from the electron beam.[29] The electronic structures of charged CNTs have been calculated by density functional theory, and it is found that the highest occupied molecular orbital (HOMO) energy of a charged CNT increases linearly with the increasing number of extra electrons, giving chances to electrons of the CNT to tunnel through a barrier near the tube wall and escape into vacuum.[30] This may be the reason that the SE emission of the CNTs is ultrahigh. Because the calculation depends on the atomic structure of CNTs, which is different from that of graphene, the effect of the electron beam on the HOMO energy may be exclusive to CNTs.

CONCLUSION

We have demonstrated experimentally that the intrinsic SE yields of monolayer graphene are around 0.10; this is comparable with the lowest yield of the ion-textured graphite that is most widely used in industry for fabricating or coating the collectors, the grids, and the envelope walls of vacuum electronic devices. But, unlike the ion-textured graphite, no post-treatment is needed for clean graphene to obtain such low SE yields. Moreover, graphene possesses lightweight, one-atom thickness, and good thermal and electrical conductivities. All of these properties meet the severe requirements of communications and space probes on weight, volume, and power consumption of the vacuum electronic devices. Therefore, it is believed that graphene has strong potential application in the fabrication of vacuum electronic devices.

EXPERIMENTAL SECTION

G1−4 were made on Si substrates by micromechanical cleavage.[1,31−33] The oxide thicknesses of the Si substrates are all 300 nm. The Raman spectra were obtained by a Renishaw 1000 Raman spectrometer with a laser of 514.5 nm. The electrodes on G1−3 were made by photolithography with the resists of PMGI SF6 from MicroChem Ltd. and S1805 G2 from Rohm and Haas Ltd., of which only PMGI SF6 contacted the graphene sheets in the lithography process, and the ones on G4 were by electron beam lithography with PMMA from MicroChem Ltd. Though the resists were different, the effects of cleaning them by the electron beam were similar to each other (see details in the Supporting Information).

The SEM examination of G1−4 was carried out using the SEM mode of a Carl Zeiss NVision 40 and its in-lens detector

exclusively for SEs. The accelerating voltage of the electron beam was 1 kV. The pressure in the SEM sample chamber was around 1×10^{-6} mbar. For each SE yield measurement, the following process was used to ensure that any influence of imaging history was avoided and the requirements of eqs 1−7 were met. Initially, we used a fast scanning speed and a low magnification to find an unused graphene. Then, we moved the graphene out of the view range and increased quickly the magnification to a high value, to ensure that the area of the view range in the next scanning would be much smaller than the total area of the graphene and the current density of the electron beam would be high. Following this, the electron beam was blanked instantly. Only after the reading of the current meter returned to zero did we unblank the electron beam and start to scan a fresh area on the oxide region beside the graphene with a scanning speed of 0.2 frames per second. This speed was much slower than the TV scanning speed that was generally a few frames per second or more.[22] During the scanning, we measured the leakage current, i'. After this measurement, we changed the working distance and repeated measuring i' on another fresh oxide area with the other conditions unchanged, until we found the working distance corresponding to $i' = 0$. Then, at this working distance, we took an SEM image of the total area of the graphene by a fast scanning speed and a low magnification. After this, we repeated the above process with slow scanning speed and high magnification on a fresh area on the graphene, such as the rectangles of X, Y, U, and W in Figures 3d and 4a, and measured i. It should be noted that the same high magnification ensured that the view range was fully covered by the graphene. After obtaining the value of i, we measured i' again on a fresh oxide area near the graphene and without any graphene, such as the rectangles of V and Z in Figure 4a, for the sake of caution.

The surface cleanliness of G1−4 and the oxide regions was checked by an AFM instrument with a Park Scientific model CP-II in the noncontact mode.

Acknowledgment. This work was supported by EPSRC (EP/H001972/1 and EP/F048009/1). J.H.W. thanks the Glasstone Fund and Brasenose College for support.

Supporting Information Available: Raman spectra, AFM images, and more SEM images of G2−4 and their analyses; AFM image of a CNT measured in our previous work[21] and its analysis. This material is available free of charge *via* the Internet at http://pubs.acs.org.

REFERENCES AND NOTES

1. Novoselov, K. S.; Geim, A. K.; Morozov, S. V.; Jiang, D.; Zhang, Y.; Dubonos, S. V.; Grigorieva, I. V.; Firsov, A. A. Electric Field Effect in Atomically Thin Carbon Films. *Science* **2004,** *306*, 666–669.
2. Geim, A. K.; Novoselov, K. S. The Rise of Graphene. *Nat. Mater.* **2007,** *6*, 183–191.
3. Du, X.; Skachko, I.; Duerr, F.; Luican, A.; Andrei, E. Y. Fractional Quantum Hall Effect and Insulating Phase of Dirac Electrons in Graphene. *Nature* **2009,** *462*, 192–195.
4. Bolotin, K. I.; Ghahari, F.; Shulman, M. D.; Stormer, H. L.; Kim, P. Observation of the Fractional Quantum Hall Effect in Graphene. *Nature* **2009,** *462*, 196–199.
5. Lin, Y.-M.; Dimitrakopoulos, C.; Jenkins, K. A.; Farmer, D. B.; Chiu, H.-Y.; Grill, A.; Avouris, Ph. 100-GHz Transistors from Wafer-Scale Epitaxial Graphene. *Science* **2010,** *327*, 662.
6. Balog, R.; Jørgensen, B.; Nilsson, L.; Andersen, M.; Rienks, E.; Bianchi, M.; Fanetti, M.; Lægsgaard, E.; Baraldi, A.; Lizzit, S.; *et al.*Bandgap Opening in Graphene Induced by Patterned Hydrogen Adsorption. *Nat. Mater.* **2010,** *9*, 315–319.
7. Zhang, J.; Xiao, J. L.; Meng, X. H.; Monroe, C.; Huang, Y. G.; Zuo, J.-M. Free Folding of Suspended Graphene Sheets by Random Mechanical Stimulation. *Phys. Rev. Lett.* **2010,** *104*, 166805.
8. Liao, L.; Lin, Y.-C.; Bao, M. Q.; Cheng, R.; Bai, J. W.; Liu, Y.; Qu, Y. Q.; Wang, K. L.; Huang, Y.; Duan, X. F. High-Speed Graphene Transistors with a Self-Aligned Nanowire Gate. *Nature* **2010,** *467*, 305–308.
9. Girit, Ç. Ö.; Meyer, J. C.; Erni, R.; Rossell, M. D.; Kisielowski, C.; Yang, L.; Park, C. -H.; Crommie, M. F.; Cohen, M. L.; Louie, S. G.;*et al.* Graphene at the Edge: Stability and Dynamics. *Science* **2009,** *323*, 1705–1708.
10. Warner, J. H.; Rümmeli, M. H.; Ge, L.; Gemming, T.; Montanari, B.; Harrison, N. M.; Büchner, B.; Briggs, G. A. D. Structural Transformations in Graphene Studied with High Spatial and Temporal Resolution. *Nat. Nano.* **2009,** *4*, 500–504.
11. Seol, J. H.; Jo, I. S.; Moore, A. L.; Lindsay, L.; Aitken, Z. H.; Pettes, M. T.; Li, X. S.; Yao, Z.; Huang, R.; Broido, D.;*et al.*Two-Dimensional Phonon Transport in Supported Graphene. *Science* **2010,** *328*, 213–216.
12. Wang, X.; Zhi, L. J.; Müllen, K. Transparent, Conductive Graphene Electrodes for Dye-Sensitized Solar Cells. *Nano Lett.* **2008,** *8*, 323–327.
13. Dayton, J. A., Jr. A Review of the Suppression of Secondary Electron Emission from the Electrodes of Multistage Collectors. NASA Technical Paper 19990028486, 1998.
14. Ding, M. Q.; Huang, M. G.; Feng, J. J.; Bai, G. D.; Yan, T. C. Ion Surface Modification for Space TWT Multistage Depressed Collectors. *Appl. Surf. Sci.* **2008,** *255*, 2196–2199.
15. Krainsky, I. L.; Vaden, K. R. Angular Distribution of Elastically Scattered Electrons Determined and Its Effect on Collector Performance Computed. NASA Technical Paper 20050188494, 2005.
16. Shih, A.; Yater, J.; Hor, C.; Abrams, R. Secondary Electron Emission Studies. *Appl. Surf. Sci.* **1997,** *111*, 251–258.
17. Graf, D.; Molitor, F.; Ensslin, K.; Stampfer, C.; Jungen, A.; Hierold, C.; Wirtz, L. Spatially Resolved Raman Spectroscopy of Single- and Few-Layer Graphene. *Nano Lett.* **2007,** *7*, 238–242.
18. Ni, Z. H.; Wang, H. M.; Kasim, J.; Fan, H. M.; Yu, T.; Wu, Y. H.; Feng, Y. P.; Shen, Z. X. Graphene Thickness Determination Using Reflection and Contrast Spectroscopy. *Nano Lett.* **2007,** *7*, 2758–2763.
19. Ferrari, A. C.; Meyer, J. C.; Scardaci, V.; Casiraghi, C.; Lazzeri, M.; Mauri, F.; Piscanec, S.; Jiang, D.; Novoselov, K. S.; Roth, S.;*et al.*Raman Spectrum of Graphene and Graphene Layers. *Phys. Rev. Lett.* **2006,** *97*, 187401.
20. Wang, Y. Y.; Ni, Z. H.; Yu, T.; Shen, Z. X.; Wang, H. M.; Wu, Y. H.; Chen, W.; Wee, A. T. S. Raman Studies of Monolayer Graphene: The Substrate Effect. *J. Phys. Chem. C* **2008,** *112*, 10637–10640.
21. Luo, J.; Warner, J. H.; Feng, C. Q.; Yao, Y. G.; Jin, Z.; Wang, H. L.; Pan, C. F.; Wang, S.; Yang, L. J.; Li, Y.;*et al.*Ultrahigh Secondary Electron Emission of Carbon Nanotubes. *Appl. Phys. Lett.* **2010,** *96*, 213113.
22. Joy, D. C.; Joy, C. S. Low Voltage Scanning Electron Microscopy. *Micron* **1996,** *27*, 247–263.
23. Martins Ferreira, E. H.; Moutinho, M. V. O.; Stavale, F.; Lucchese, M. M.; Capaz, R. B.; Achete, C. A.; Jorio, A. Evolution of the Raman Spectra from Single-, Few-, and Many-Layer Graphene with Increasing Disorder. *Phys. Rev. B* **2010,** *82*, 125429.
24. Kanaya, K.; Kawakatsu, H. Secondary Electron Emission Due to Primary and Backscattered Electrons. *J. Phys. D* **1972,** *5*, 1727–1742.
25. Kanaya, K.; Ono, S.; Ishigaki, F. Secondary Electron Emission from Insulators. *J. Phys. D* **1978,** *11*, 2425–2437.
26. Joy, D. C.; Joy, C. S. Dynamic Charging in the Low Voltage SEM. *Microsc. Microanal.* **1995,** *1*, 109–112.
27. Joy, D. C. A. Database on Electron-Solid Interactions. *Scanning* 1995, *17*, 270−275. Data available at http://web.utk.edu/∼srcutk/htm/interact.htm.
28. Finnie, P.; Kaminska, K.; Homma, Y.; Austing, D. G.; Lefebvre, J. Charge Contrast Imaging of Suspended Nanotubes by Scanning Electron Microscopy. *Nanotechnology* **2008,** *19*, 335202.
29. Nojeh, A.; Shan, B.; Cho, K.; Pease, R. F. W. *Ab Initio* Modeling of the Interaction of Electron Beams and Single-Walled Carbon Nanotubes. *Phys. Rev. Lett.* **2006,** *96*, 056802.
30. Luo, J.; Peng, L. -M.; Xue, Z. Q.; Wu, J. L. Density-Functional-Theory Calculations of Charged Single-Walled Carbon Nanotubes. *Phys. Rev. B* **2002,** *66*, 115415.

31. Novoselov, K. S.; Jiang, D.; Schedin, F.; Booth, T. J.; Khotkevich, V. V.; Morozov, S. V.; Geim, A. K. Two-Dimensional Atomic Crystals. *P. Natl. Acad. Sci. U. S. A.* **2005,** *102*, 10451–10453.
32. Nair, R. R.; Blake, P.; Grigorenko, A. N.; Novoselov, K. S.; Booth, T. J.; Stauber, T.; Peres, N. M. R.; Geim, A. K. Fine Structure Constant Defines Visual Transparency of Graphene. *Science* **2008,** *320*, 1308.
33. Ling, X.; Xie, L. M.; Fang, Y.; Xu, H.; Zhang, H. L.; Kong, J.; Dresselhaus, M. S.; Zhang, J.; Liu, Z. F. Can Graphene Be Used As a Substrate for Raman Enhancement? *Nano Lett.* **2010,** *10*, 553–561.